RSC Advances




ROYAL SOCIETY OF CHEMISTRY

www.rsc.org/advances

# Electrochemical detection of nitrite based on glassy carbon electrode modified with gold-polyaniline-graphene nanocomposites

Xuemei Ma[a], Tingting Miao[b], Wencai Zhu[a], Xiaochun Gao[a], Chuntao Wang[c], Caicai Zhao[a], Houyi Ma[a,*]

[a] *Key Laboratory for Colloid and Interface Chemistry of State Education Ministry, School of Chemistry and Chemical Engineering, Shandong University, Jinan 250100, China*

[b] *State Key Laboratory of Crystal Materials, Shandong University, Jinan 250100, China*

[c] *Department of Chemistry, Taiyuan Normal University, Taiyuan 030031, China*

*Corresponding author.

Tel: +86-531-88364959; Fax: +86-531-88564464; E-mail: hyma@sdu.edu.cn

**Abstract**

First, the polyaniline-graphene oxide (GO-PANI) nanocomposites were prepared by in situ polymerization of aniline in the presence of graphene oxide (GO). Next, the GO-PANI nanocomposites were reduced to polyaniline-graphene (G-PANI) nanocomposites by a green electrochemical reduction method. Finally, a thin layer of nearly monodispersed Au nanoparticles with uniform size (~ 12 nm) was coated on the surface of G-PANI nanocomposites. Moreover, the as-prepared Au-polyaniline-graphene (Au-G-PANI) nanocomposites can be used as the sensing electrode materials for the electrochemical detection of nitrite ($NO_2^-$). As compared with other common modified electrodes, the Au-G-PANI/GCE shows an obvious oxidation peak of $NO_2^-$ with the larger peak current, and gives a wider linear range from 0.1 to 200 μmol/L, with the detection limit of 0.01 μmol/L (S/N = 3). Besides, the oxidation process of $NO_2^-$ on the Au-G-PANI/GCE is proved to be a surface-controlled process involving the transfer of two electrons. The present study widens the application of graphene-based nanocomposite materials in the electrochemical detection of environmental pollutants.

***Keywords:*** *Gold; Graphene; Polyaniline; Nitrite; Amperometry*

**Introduction**

Nitrite ($NO_2^-$) is extensively used in dye synthesis, food industry and corrosion inhibition. It is also an essential precursor in the formation of nitrosamines, which is a strong carcinogen to human bodies [1,2]. Once the $NO_2^-$ is taken too much, the capability of hemoglobin that binds oxygen would decrease significantly since $NO_2^-$ can oxidize ferrohemoglobin to ferrihemoglobin [3]. The World Health Organization (WHO) has clearly regulated that the content of $NO_2^-$ in raw water cannot exceed 3 mg/L [4]. Therefore, the simple and effective determination of $NO_2^-$ is of great significance in public health. Up to now, many techniques have been developed to determine $NO_2^-$ levels, such as spectrophotometry [5], ion chromatography [6], gas chromatography-mass spectrometry [7], high-performance liquid chromatography [8], chemiluminescence [9], capillary electrophoresis [10] and electrochemical methods [11-13]. Among them, electrochemical methods have attracted considerable attention by virtue of fast response, simple operation, high sensitivity and excellent selectivity.

Generally, the electrochemical determination of $NO_2^-$ previously reported is carried out by either oxidation or reduction of $NO_2^-$. However, seeing that the reduction process of $NO_2^-$ is quite complicated, involving a series of intermediate products [14–16], the studies concerning the electrochemical oxidation of $NO_2^-$ have attracted more attention in recent years. At present, the challenge that researchers face is that the intermediate species generating during the oxidation of $NO_2^-$ may contaminate the electrode surface and decrease the sensitivity and accuracy of the electrodes used [17], and the application of bare glassy carbon electrode (GCE) in the $NO_2^-$ detection is limited to a considerable degree. To overcome the difficulties, some novel nanostructured materials with large surface area and excellent catalytic activity, such as Au@$Fe_3O_4$ nanoparticles [18], gold nanoparticles/poly(3-methylthiophene) composites [19], and graphene/polypyrrole/chitosan nanocomposite [20], have been applied to modify the commercial GCEs.

Polyaniline, a kind of typical conductive polymer, has received increased interest due to its high electrical conductivity, good environmental stability and simple synthesis. These outstanding characteristics enable polyaniline to be applied in many fields including catalysis [21], corrosion protection [22], supercapacitor [23] and sensors [24,25]. On the other hand, Au nanoparticles,

owing to the excellent conductivity and catalytic property, have been extensively used in analytical electrochemistry. In addition, the existing results have shown that Au nanoparticles possess excellent catalytic performance for electrochemical oxidation of $NO_2^-$ [26,27].

We have noticed that, the graphene-metal nanocomposites, which combine the good conductivity and high specific surface area of 2D graphene with the catalytic activity of 0D metal nanoparticles, have attracted much attention in the fabrication of electrochemical sensors. In this paper, we synthesized Au-G-PANI nanocomposites at first, and then constructed the nitrite sensing electrodes by using the as-prepared Au-G-PANI nanocomposites to modify the GCEs. The as-fabricated sensing electrodes (Au-G-PANI/GCEs) exhibited good response towards the oxidation of $NO_2^-$. Both cyclic voltammetry (CV) and rotating disk electrode techniques were also employed to collect kinetic data for the oxidation of $NO_2^-$ on the Au-G-PANI/GCE. It is expected that the electrochemical sensors based on Au-G-PANI/GCE will find wide applications in practical monitoring of $NO_2^-$.

**Scheme 1.**

## 2. Experimental

### 2.1 Reagents and apparatus

Sodium nitrite, aniline and chloroauric acid ($HAuCl_4 \cdot 3H_2O$) were purchased from Sinopharm Chemical Reagent Co. Ltd. (Shanghai, China). All chemicals (analytical grade) were used without further purification. All of the solutions were prepared with ultrapure water (~ 18 MΩ cm). The 0.1 mol/L phosphate buffer solution (PBS) was employed as a supporting electrolyte.

All CV measurements were performed with a CHI 650A electrochemical workstation (Shanghai Chenhua Instrument Company, China) at room temperature (~ 25 ºC) in a conventional three-electrode cell. A rotating disk electrode (RDE, Pine Instrumentation) was used as the working electrode to obtain the hydrodynamic voltammograms for the oxidation of $NO_2^-$. For conventional electrochemical measurements, the modified GCE (Φ = 5 mm) was selected as the working electrode, and a bright Pt plate with a surface area of 4 $cm^2$ and a saturated calomel electrode (SCE) served as the counter electrode and the reference electrode, respectively. The reference

electrode was led to the surface of the working electrode through a Luggin capillary. All potentials presented in this paper were referred to SCE. The electrolyte solutions were deoxygenated by $N_2$ bubbling for 10 min prior to electrochemical measurements and a blanket of $N_2$ was maintained throughout each experiment.

Considering that electrochemical impedance spectroscopy (EIS) is an effective tool for probing the interfacial charge-transfer kinetics [28], EIS measurements were carried out with an ACM electrochemical workstation at the open circuit potentials in 0.10 mol/L KCl with 5 mmol/L $Fe[(CN)_6]^{3-/4-}$. The frequency range was chosen between 100 kHz and 0.1 Hz, and AC voltage amplitude was 5 mV.,

The morphologies and structures of the nanocomposites were characterized by high-resolution transmission electron microscope (JEM-2100, Japanese electronics Co. Ltd, Japan).

2.2 Preparation of GO-PANI nanocomposites and nanostructured Au films

Graphene oxide (GO) was synthesized from natural graphite powder using a modified Hummers method [29], and GO-PANI nanocomposites were prepared via an improved procedure based on the previous synthetic method [30]. The synthesis process of GO-PANI nanocomposites was described as follows: 0.55 mL of aniline was firstly dissolved in 20 mL of 1 mol/L dilute HCl to form a homogeneous solution, then 30 mg GO was dispersed in the aniline solution with the help of ultrasonication. Immediately afterwards, 0.3422 g $(NH_4)_2S_2O_8$ was dissolved in 10 mL of 1 mol/L dilute HCl, and the resulting solution was poured into the acidic solution containing aniline and GO. Under strong stirring conditions, the polymerization reaction took place quickly and the color of bulk solution turned green. The stirring was kept for overnight so that the reaction could be carried out adequately. After the completion of the reaction, the mixed solution is diluted by adding 75 mL ultrapure water. Subsequently, the resulting dispersion was centrifuged, washed with ethanol, and finally dried in drying oven at 60 ºC overnight.

The preparation of nanostructured gold film is carried out according to the method described previously [31]. Au nanoparticles were synthesized by using citrate to reduce chloroauric acid in water phase. In order to acquire a freestanding thin film, 20 mL of Au nanoparticle dispersion and 5 mL of butanol or pentanol were continuously poured into an evaporating dish. The nanoparticles

began to self-assemble spontaneously and formed the monolayer films at the oil-water interface. This process could be accelerated by a slight vibration or adding 1.25 mL of ethanol to the mixed solution. Subsequently, the mixed solution was heated to 48□ in water bath and then kept at the temperature for 3 h, and finally dried at room temperature for one day. The as-prepared films could be picked up by a copper coil.

2.3 Preparation of the modified electrodes

The GO-PANI suspension was prepared by dispersing 1 mg GO-PANI in 1 mL DMF solution for 2 h with the aid of sonication. Prior to modification, GCE was carefully polished to a mirror-like surface with 1.0 μm, 0.3 μm and 0.05 μm α-alumina powders in sequence, rinsed thoroughly with pure water after each polishing step, sonicated in nitric acid (1:1) and pure water for 5 min respectively, and dried in nitrogen atmosphere. Then 10 μL GO-PANI dispersion was dropped onto the surface of a clean GCE, followed by drying in an infrared lamp to form GO-PANI/GCE. The G-PANI/GCE was obtained by electrochemical reduction of a freshly prepared GO-PANI/GCE in 20 mmol/L $NaH_2PO_4$ at -0.75 V for 10 min. A layer of Au nanoparticle film was placed on the surface of G-PANI/GCE with copper coils, followed by drying naturally at room temperature to form Au-G-PANI/GCE.

Before each electrochemical test, the Au-G-PANI/GCE was washed repeatedly with ultrapure water, and then activated by carrying out four voltammetric cycles within the potential range of 0-1.55 V in 0.5 mol/L $H_2SO_4$.

**3. Results and discussion**

3.1 Characterization of GO-PANI nanocomposites and nanostructured Au films

Morphological and structural features of GO, GO-PANI and Au nanoparticles were characterized by means of TEM. As shown in Fig.1A, the typical TEM image of GO shows the nearly transparent sheets with large plane size. The approximately transparent appearance indicates that GO is very thin and only made of several layers of carbon atoms, which is consistent with the

results reported in previous literatures [32,33]. Upon the addition of aniline solution, the surface of GO is covered with a very thin layer of polyaniline (Fig.1B). However, the wrinkle-shaped structure still can be seen, which indicates the surface morphology of GO sheets almost keeps unchanged [34]. The typical TEM images of Au nanoparticles show that Au nanoparticles are around 12 nm in size and nearly monodispersed (Fig.1 C, D). The small size and good uniformity of Au nanoparticles are conducive to enhancing the electrocatalytic activity.

**Fig.1**

Fig. 2 shows the FTIR spectra of GO, GO-PANI and GO-PANI. The FTIR spectrum of GO (curve a) shows the broad and intense O-H peak at 3400 $cm^{-1}$, C=O peak at 1730 $cm^{-1}$, C=C peak at 1620 $cm^{-1}$, and C-O stretching peak at 1065 $cm^{-1}$. As shown in Figure 2b, for the GO-PANI sample, the peak in the wavenumber range of 3200-3500 $cm^{-1}$ is attributable to the N-H stretching vibrations. The weak shoulder peaks at 2900-3050 $cm^{-1}$ correspond to aromatic $sp^2$ C-H stretching. The peaks at 1302 and 1140 $cm^{-1}$ correspond to C-N stretching of the secondary aromatic amine and C=N stretching, respectively. These results confirm that PANI has been polymerized on the surface of GO. After the GO-PANI was electrochemically reduced (curve c), the C=O (1730 $cm^{-1}$) and C–O (1065 $cm^{-1}$) vibration bands disappeared, which confirms that GO-PANI has been reduced by using the electrochemical approach. The peaks between 1100 and 1660 $cm^{-1}$ are associated with the stretching vibrations of C-N and C-C bonds, and the stretching of C-H bonds.

**Fig.2**

3.2 Electrochemical behavior of the modified electrodes

By using 5 mmol/L $Fe(CN)_6^{3-/4-}$ couple (1:1) as the redox probe and employing the modified GCE as the working electrode, we firstly investigated the charge-transfer rates at the solution/electrode interface in 0.25 mol/L KCl solution. As seen in Fig.3A, The cyclic voltammograms (CVs) of a bare GCE (curve a) show a pair of broad redox peaks with $\Delta E_p$ of 210 mV. But when the GCE was modified with G-PANI, the CVs of the G-PANI/ GCE (curve b) displayed the higher peak currents and smaller $\Delta E_p$ value. The difference between the two CV curves (a and b) can be attributed to the larger surface area of G, the faster electron-transfer rate at the interface and the

better electrical conductivity of the G-PANI. Furthermore, when the GCE was modified with Au-G-PANI nanocomposites, the CVs (curve c) of the as-obtained Au-G-PANI /GCE was very similar to those (curve b) of the G-PANI/GCE mentioned above.

Fig.3B shows a set of Nyquist impedance spectra of bare GCE and modified GCEs. Based on the $R_{ct}$ values of the three electrodes, the bare GCE shows the largest charge-transfer resistance ($R_{ct}$ = 690.2 Ω, Spectrum a), indicating the slowest charge-transfer rate at the electrode/solution interface. But when the GCE was modified with G-PANI, the charge-transfer resistance decreased obviously ($R_{ct}$ = 166.8 Ω, Spectrum b). This confirms that G-PANI was excellent electric conducting material and could accelerate the electron transfer rate [35]. It is worth mentioning that, the Au-G-PANI/GCE shows the slightly greater charge-transfer resistance ($R_{ct}$ = 270.2 Ω, Spectrum c) than the G-PANI/GCE, which is perhaps associated with the fact that the deposition of Au nanoparticles on the electrode surface formed a blocking layer for the transport of ferrocyanide ions [36]. This also implies from one side that the monodisperse Au nanoparticles have been successfully attached onto the surface of G-PANI.

**Fig.3**

3.3 Voltammetric behavior of $NO_2^-$

The oxidation of $NO_2^-$ at the bare GCE and the modified GCEs were studied in 0.10 mol/L PBS by means of the CV method. As can be seen in Fig.4, there are no obvious oxidation peaks at the bare GCE and G-PANI/GCE (see curves a and b), indicating that the bare GCE and G-PANI/GCE are unable to catalyze the electrochemical oxidation reaction of $NO_2^-$. However, the CVs of Au/GCE and Au-G-PANI/GCE show obvious oxidation peaks (see curves c and d), with the oxidation peak potential being around 0.78 V. This phenomenon implies that Au nanoparticles possess strong electrocatalytic activity towards the electrochemical oxidation reaction of $NO_2^-$. Furthermore, the anodic peak current recorded on the Au-G-PANI/GCE was observed to increase significantly, about three times as large as the value recorded on the Au/GCE. Through above comparison and analysis, it is not difficult to draw a conclusion that the Au-G-PANI exhibits the enhanced electrocatalytic performance. The main reason is that such electrode combines advantages of G-PANI/GCE and Au nanoparticles, including large surface area, excellent conductivity and good

catalytic activity.

**Fig.4**

3.4 Effect of pH

The influence of pH values on the oxidation of $NO_2^-$ at the Au-G-PANI/GCE was studied by means of differential pulse voltammetry (DPV) in 0.10 mol/L PBS within the pH range of 4.0-6.0. As indicated in Fig.5A, the peak current corresponding to the oxidation of $NO_2^-$ increased with the increase of pH value until the pH value reached 5.0, and then began to decreased obviously with the further increase of pH value (see Fig. 5B). As we all know, the $NO_2^-$ is not stable in strong acidic media and can undergo the following transformation [37]:

$$2H^+ + 3NO_2^- \rightarrow 2NO + NO_3^- + H_2O$$

On the other hand, most nitrite anions are protonated in acidic solution because the $pK_a$ of $HNO_2$ is 3.3 [38]. Protonation was proved to be involved in the catalytic reaction process. Thus, in this case the electrochemically active species should be $HNO_2$ rather than $NO_2^-$ [39]. When the pH is greater than 5.0, the electrocatalytic oxidation of nitrite will become more difficult due to the shortage of protons [39], so the peak current will naturally decrease. And moreover, a $–NH_2$ group was converted into a non-nucleophilic amine ($–NH_3^+$) in the case of lower pH values, which made it easy to absorb $NO_2^-$ [40]. Therefore, the PBS of pH 5.0 was selected as the optimum electrolyte in electrochemical detection of nitrite.

**Fig.5**

3.5 Effect of scan rate

The influence of scan rates on the oxidation behavior of $NO_2^-$ at Au-G-PANI/GCE was investigated by using CV method. Fig.6A indicates the peak currents increase continuously with the increase of scan rates in the range of 10-1000 mV/s. Moreover, there is a linear relationship between the peak current ($I_p$) and the scan rate ($v$) (Fig.6B), indicating that the oxidation process of $NO_2^-$ is a typical surface-controlled process. The fitted regression equation can be expressed as follows:

$$I_p\ (\mu A) = 4.768 + 0.00999v \quad (v\text{: mV/s})\ (R^2 = 0.9968) \tag{1}$$

Moreover, it is observed that, the oxidation peak potential ($E_p$) shift to more positive potentials with the increase of scan rate, leading to a linear relationship between $E_p$ and log$v$ (Fig.6C). The regression equation is given below:

$$E_p = 0.7358 + 0.03156\log v \quad (v\text{: mV/s})\ (R^2 = 0.9964) \tag{2}$$

which confirms the irreversibility for the electrocatalytic oxidation process of $NO_2^-$.

For an irreversible process, the $E_p$ can be represented by the following equation [41]:

$$E_p = b/2\log v + A \tag{3}$$

where b = Tafel slope = 2.303RT/(1−$\alpha$)nF; A is a constant, being associated with the formal electrode potential ($E_0$) and standard rate constant at $E_0$; R, T and F are the gas constant, temperature and Faraday constant respectively; $\alpha$ is the charge transfer coefficient, characterizing the effect of electrochemical potential on activation energy of an electrochemical reaction; n is the number of electrons involved in the rate-determining step. Based on the slope value obtained from Fig.6C, the value of (1−$\alpha$)n can be calculated with ease. Assuming that n = 2, the value of $\alpha$ was calculated to be 0.5316 according to Eq.(3), being close to the theoretical value of 0.5 [42]. This shows a fact that there is an equal probability that the activated transition state can form either products or reactants [43]. Thus, we may assume that the electrocatalytic response of $NO_2^-$ at Au-G-PANI/GCE follows the following mechanism [44]:

$$NO_2^- + H_2O \rightarrow NO_3^- + 2H^+ + 2e$$

**Fig.6**

3.6 Hydrodynamic study with rotating disk electrode

The reaction process of $NO_2^-$ at Au-G-PANI/GCE can be further studied by using hydrodynamic voltammetry at a rotating disk electrode (RDE). As shown in Fig.7A, a set of hydrodynamic voltammetry curves were recorded on Au-G-PANI/GCE RDE with 0.10 mmol/L $NO_2^-$. It can be seen that the peak currents increase continuously with the increase of rotation rates (ω) in the range of 300-3000 rpm. According to the Koutecky-Levich plots [45]:

$$i_l = 0.62nFAD^{2/3}C^*\upsilon^{-1/6}\omega^{1/2} \tag{4}$$

If the limiting current ($i_l$) is proportional to the square root of rotation rates ($\omega^{1/2}$), the reaction taking place on the RDE is totally mass-transfer-limited. However, as seen in Fig.7B, there is not a

good linear relationship between $i_l$ and $\omega^{1/2}$, suggesting that the reaction process of $NO_2^-$ at Au-G-PANI/GCE is not limited absolutely by kinetics. Considering that the electron transfer rate between Au-G-PANI and GCE is very fast, the oxidation of $NO_2^-$ on Au-G-PANI could be controlled by a mixed process. Thus, the Koutecky–Levich [45] can be applied to this condition:

$$\frac{1}{i_l} = \frac{1}{nFAk\ \Gamma C^*} + \frac{1}{0.62\, nFAD^{\ 2/3} C^* \nu^{-1/6} \omega^{1/2}} \qquad (5)$$

As shown in Fig.7C, there exists a linear relationship between $i_l^{-1}$ and $\omega^{-1/2}$ ($R^2$ = 0.9968), implying that the oxidation process of $NO_2^-$ at Au-G-PANI/GCE is controlled by the mixed process.

**Fig.7**

3.7 Amperometric detection of $NO_2^-$

A typical current-time response curve for the successive addition of $NO_2^-$ in stirred 0.10 mol/L PBS (pH 5.0) at the applied potential of +0.80 V was shown in Fig.8. A well-defined and fast amperometric response was observed under the above-mentioned condition. The detection range of $NO_2^-$ was determined to be 0.1-200 μmol/L. The inset shown in the Fig.8A presents a calibration curve for the steady state current versus $NO_2^-$ concentrations. The fitting regression equation was given as follows:

$$I_p\ (\mu A) = 0.1453 + 0.1066\ C_{NO2}^-\ (\mu mol/L) \quad (R^2 = 0.9986) \qquad (6)$$

The limit of detection is 0.01 μmol/L (S/N = 3). These results indicate that the sensing electrodes based on Au-G-PANI nanocomposites are very applicable to the electrochemical determination of $NO_2^-$, with a lower detection limit and a wider detection range compared to other modified electrodes (see Table 1).

When the concentration of $NO_2^-$ increased to more than 200 μmol/L, the current response was not proportional to the concentration of $NO_2^-$ and showed a tendency to become a plateau. Because the valence of nitrogen in the $NO_2^-$ is +3, an intermediate valence state, the $NO_2^-$ can be either oxidized or reduced. Thus, disproportionation and decomposition of $NO_2^-$ can happen at the same time. The former may generate nitric oxide and nitric acid, while the latter can form nitric oxide and nitrogen dioxide. This implies that the adsorption of the intermediate species has an adverse impact on the sensitivity of the modified electrodes.

**Fig.8**

**Table 1**

3.8 Reproducibility, stability and anti-interference performance

The reproducibility of Au-G-PANI/GCE was investigated in 0.10 mol/L PBS (pH 5.0) containing 10 μmol/L $NO_2^-$ by means of DPV method. By continuously recording the response current to $NO_2^-$, the relative standard deviation (RSD) for 10 successive measurements of $NO_2^-$ at the same Au-G-PANI/GCE was determined to be 3.9%. The reproducibility of the developed method was also evaluated by using five different Au-G-PANI/GCEs in 0.10 mol/L PBS (pH 5.0) with 10 μmol/L $NO_2^-$, and the resulting RSD was about 5.1%. Furthermore, the stability of the Au-G-PANI/GCE was investigated by measuring the current response after the modified electrode was stored at 4 ºC for a month. The current responses still retained more than 90% of the initial response. It is evident that the modified electrodes present good reproducibility and stability for the $NO_2^-$ determination.

The modified electrode can be cleaned easily and reused by continuous CV scanning in the blank solution. Possible interferences for the detection of $NO_2^-$ on the Au-G-PANI/GCE were investigated by adding various foreign species into 0.10 mol/L PBS (pH 5.0) containing 0.10 mmol/L $NO_2^-$. It is found that the addition of 100-fold concentration of $Na^+$, $K^+$, $Co^{2+}$, $Ni^{2+}$, $Cu^{2+}$, $Fe^{3+}$, $Cl^-$, $NO_3^-$ , $SO_4^{2-}$ and 20-fold ascorbic acid, uric acid caused no obvious current response (< 5% of current change). These results demonstrate that the as-prepared electrochemical sensor has excellent anti-interference ability.

**Conclusions**

A facile electrochemical reduction method was developed to synthesize polyaniline-graphene (G-PANI) nanocomposites, and a thin layer of nearly monodispersed Au nanoparticles with uniform size (around 12 nm) was coated on the surface of G-PANI. Moreover, the nitrite electrochemical sensor based on Au-G-PANI nanocomposites was fabricated by using the as-prepared nanocomposites to modify glassy carbon electrode (GCE). The CVs of the

Au-G-PANI/GCE show an obvious oxidation peak and significantly enhanced peak currents for the oxidation reactions of $NO_2^-$, which is due to the fact that Au-G-PANI nanocomposites combine the advantages of large surface area and extraordinary electronic transport property of G-PANI with the catalytic property of Au nanoparticles. The Au-G-PANI/GCE also presents low detection limit and wide linear range. Thus, the Au-G-PANI nanocomposites may be a promising electrochemical sensor material for the high sensitivity detection of certain environmental pollutants in the near future.

**Acknowledgements**

This work was supported by the National Research Foundation for the Doctoral Program of Higher Education of China (20120131110009) and the National Natural Science Foundation of China (21373129, 21175059).

**Reference**

[1] W. Lijinsky, S.S. Epstein, *Nature*, 1970, **225**, 21-23.

[2] S.S. Mirvish, *Cancer Lett.*, 1995, **93**, 17-48.

[3] C. S. Bruning, J. B. Kaneene, *Vet. Hum. Toxicol.*, 1993, **35**, 521-538.

[4] Guide lines for Drinking-Water Quality (3 rd edn), vol. 1, World Health Organization, Geneva, 2004.

[5] I. A. Tsoulfanidis, G. Z. Tsogas, D. L. Giokas, A. G. Vlessidis, *Microchim. Acta*, 2008, **160**, 461-469.

[6] C. Abha, K. B. Anil, V. K. Gupta, *Talanta*, 2001, **55**, 789-797.

[7] S. M. Helmke, M. D. Duncan, *J. Chromatogr. B*, 2007, **851**, 83-92.

[8] V. D. Matteo, E. Esposito, *J. Chromatogr. A*, 1997, **789**, 213-219.

[9] A. Lagalante, P. Greenbacker, *Anal. Chim. Acta*, 2007, **590**, 151-158.

[10] J. H. Wang, W. H. Huang, Y. M. Liu, J. K. Cheng, J. Yang, *Anal. Chem.*, 2004, **76**, 5393-5398.

[11] R. Yue, Q. Lu, Y. K. Zhou, *Biosens. Bioelectron.*, 2011, **26**, 4436-4441.

[12] O. Brylev, M. Sarrazin, L. Roue, D. Belanger, *Electrochim. Acta*, 2007, **52**, 6237-6247.

[13] Q. P. Chen, S. Y. Ai, X. B. Zhu, H. S. Yin, Q. Ma, Y. Y. Qiu, *Biosens. Bioelectron.*, 2009, **24**, 2991-2996.

[14] J. Li, X. Q. Lin, *Microchem. J.*, 2007, **87**, 41-46.

[15] W. W. Yang, Y. Bai, Y. C. Li, C. Q. Sun, *Anal. Bioanal. Chem.*, 2005, **382**, 44-50.

[16] M. Li, P. He, Y. Zhang, N. Hu, *Biochim. Biophys. Acta*, 2005, **1749**, 43-51.

[17] B. R. Kozub, N. V. Rees, R. G. Compton, *Sens. Actuators, B*, 2010, **143**, 539-546.

[18] C. M. Yu, J. W. Guo, H. Y. Gu, *Electroanal.*, 2010, **22**, 1005-1011.

[19] X. Huang, Y. X. Li, Y. L. Chen, L. Wang, *Sens. Actuators, B*, 2008, **134**, 780-786.

[20] D. X. Ye, L. Q. Luo, Y. P. Ding, Q. Chen, X. Liu, *Analyst*, 2011, **136**, 4563-4569.

[21] A. H. Gemeay, R. G. El-Sharkawy, I. A. Mansour, A. B. Zaki, *J. Colloid Interface Sci.*, 2007, **308**, 385-394.

[22] J. M. Yeh, S. J. Liou, C. Y. Lai, P. C. Wu, *Chem. Mater.*, 2001, **13**, 1131-1136.

[23] Y. Zhou, Z. Y. Qin, L. Li, Y. Zhang, Y. L. Wei, L. F. Wang, M. F. Zhu, *Electrochim. Acta*, 2010, **55**, 3904-3908.

[24] J. D. Qiu, L. Shi, R. P. Liang, G. C. Wang, X. H. Xia, *Chem. Eur. J.*, 2012, **18**, 7950-7959.

[25] J. D. Huang, Q. Lin, X. M. Zhang, X. R. He, X. R. Xing, W. J. Lian, M. M. Zuo, Q. Q. Zhang, *Food Res. Int.*, 2011, **44**, 92-97.

[26] B. Q. Yuan, C. Y. Xu, L. Liu, Y. F. Shi, S. J. Li, R. C. Zhang, D. J. Zhang, *Sens. Actuators, B*, 2014, **198**, 55-61.

[27] A. Abbas, S. F. Farzaneh, M. Tayyebeh, G. Hamed, *Biosens. Bioelectron.*, 2014, **51**, 379-385.

[28] F. Patolsky, M. Zayats, E. Katz, I. Willner, *Anal. Chem.*, 1999, **71**, 3171-3180.

[29] W. S. Hummers, R. E. Offeman, *J. Am. Chem. Soc.*, 1958, **80**, 1339-1339.

[30] K. Zhang, L. L. Zhang, X. S. Zhao, J. S. Wu, *Chem. Mater.*, 2010, **22**, 1392-1401.

[31] H. B. Xia, D. Y. Wang, *Adv. Mater.*, 2008, **20**, 4253-4256.

[32] Y. C. Si, E. T. Samulski, *Nano Lett.*, 2008, **8**, 1679-1682.

[33] A. Ambrosi, Z. Sofer, J. S. Cross, M. Pumera, *Chem. Eur. J.*, 2011, **17**, 10763-10770.

[34] D. W. Wang, F. Li, J. P. Zhao, W. C. Ren, Z. G. Chen, J. Tan, Z. S. Wu, I. Gentle, G. Q. Lu, H. M. Cheng, *ACS Nano*, 2009, **3**, 1745-1752.

[35] S. Liu, X. R. Xing, J. H. Yu, W. J. Lian, J. Li, M. Cui, J. D. Huang, *Biosens. Bioelectron.*, 2012, **36**, 186-191.

[36] Q. L. Sheng, M. Z. Wang, J. B. Zheng, *Sens. Actuators, B*, 2011, **160**, 1070-1077.

[37] O. Brylev, M. Sarrazin, L. Roué, D. Bélangér, *Electrochim. Acta*, 2007, **52**, 6237–6247.

[38] G. Milczarek, *J. Electroanal. Chem.*, 2007, **610**, 199–204.

[39] X. Huang, Y. X. Li, Y. L. Chen, L. Wang, *Sens. Actuators B*, 2008, **134**, 780–786.

[40] L. Y. Jiang, R. X. Wang, X. M. Li, L. P. Jiang, G. H. Lu, *Electrochem. Commun.*, 2005, **7**, 597-601.

[41] E. Laviron, L. Roullier, *Electroanal. Chem.*, 1980, **115**, 65-74.

[42] J. N. Soderberg, A. C. Co, A. H. C. Sirk, V. I. Birss, *J. Phys. Chem. B*, 2006, **110**, 10401-10406.

[43] B. O. Agboola, T. Nyokong, *Anal. Chim. Acta*, 2007, **587**, 116-123.

[44] Q. Wang, Y. B. Yun, *Microchim. Acta*, 2012, **177**, 411-418.

[45] A. J. Bard, L. R. Faulkner, *Electrochemical methods, fundamentals and applications*, 1980, 226-236.

**Figure caption**

**Scheme 1.** Scheme diagram of the $NO_2^-$ sensor based on the modified electrode.

**Fig.1** TEM images of GO (A), GO-PANI (B) and Au nanoparticles (C, D).

**Fig. 2** FTIR spectras of GO (a), GO-PANI (b) and G-PANI (c).

**Fig.3** (A) CVs of GCE (a), G-PANI/GCE (b) and Au-G-PANI/GCE (c) in 0.1 mol/L KCl containing 5 mmol/L $Fe[(CN)_6]^{3-/4-}$. (B) Nyquist plots of GCE (a), G-PANI/GCE (b) and Au-G-PANI/GCE (c) in 0.10 mol/L KCl containing 5 mmol/L $Fe[(CN)_6]^{3-/4-}$, and the inset shows the Randles equivalent circuit.

**Fig.4** CVs of GCE (a), G-PANI/GCE (b), Au/GCE (c) and Au-G-PANI/GCE (d) in 0.10 mol/L PBS with 0.10 mmol/L $NO_2^-$.

**Fig.5** (A) DPVs of Au-G-PANI/GCE in 0.10 mol/L PBS containing 0.10 mmol/L $NO_2^-$ at different pH values. (B) The relationship between the oxidation peak currents and the pH values.

**Fig.6** (A) CVs of Au-G-PANI/GCE in 0.10 mol/L PBS (pH 5.0) containing 0.10 mmol/L $NO_2^-$ at different scan rates. (B) The linear dependence of $I_p$ on $v$. (C) The linear dependence of $E_p$ on log$v$.

**Fig.7** (A) DPVs of Au-G-PANI/GCE RDE in 0.10 mol/L PBS (pH 5.0) containing 0.10 mmol/L $NO_2^-$ at different rotation rates. (B) The linear dependence of $i_l$ on $\omega^{1/2}$. (C) The linear dependence of $i_l^{-1}$ on $\omega^{-1/2}$.

**Fig.8** (A) Amperometric response obtained on the Au-G-PANI/GCE with the increasing $NO_2^-$ concentration. Inset: The dependence of the current response on the concentration of $NO_2^-$. (B) The current response to low concentration $NO_2^-$ on Au-G-PANI/GCE. Supporting electrolyte: 0.10 mol/L PBS (pH 5.0), applied potential: +0.80 V.

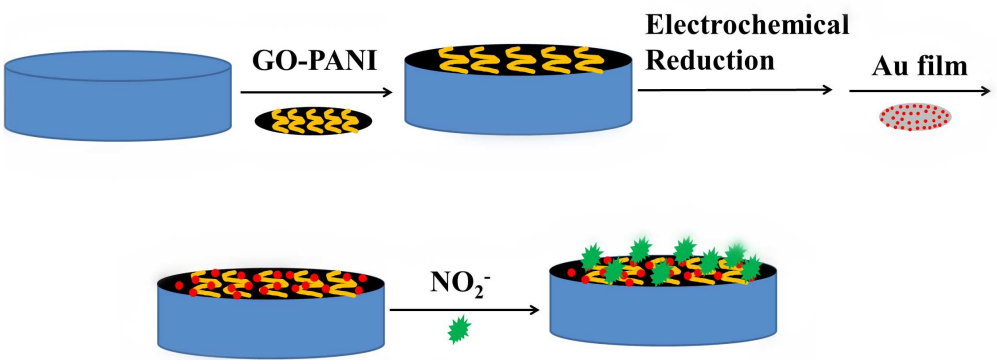


**Scheme 1.** Scheme diagram of the $NO_2^-$ sensor based on the modified electrode.

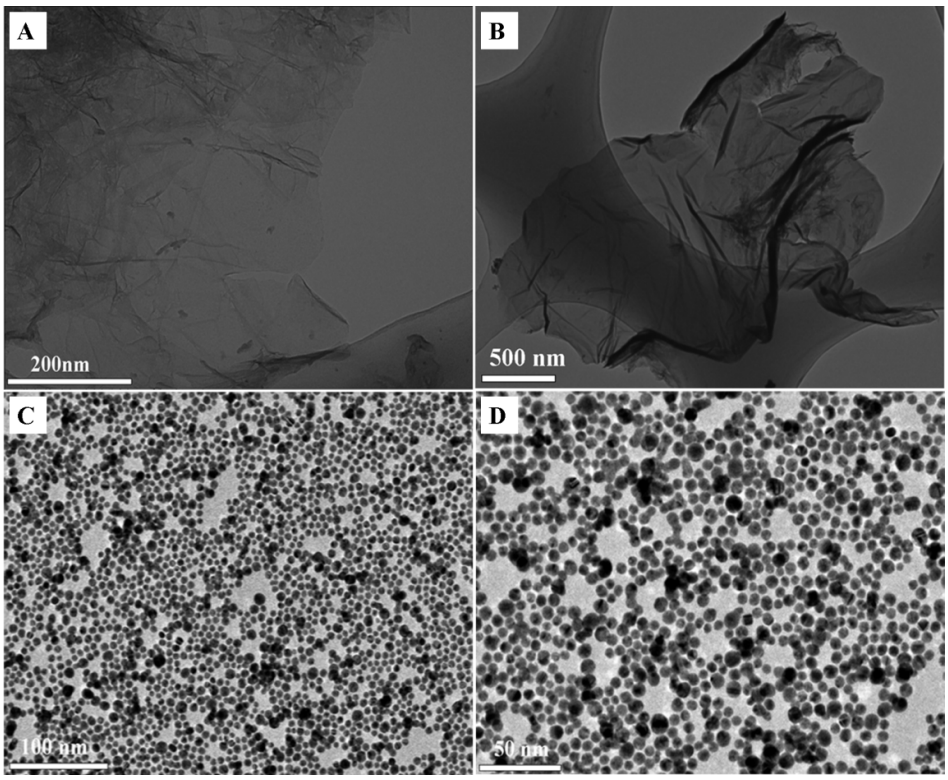


**Fig.1** TEM images of GO (A), GO-PANI (B) and Au nanoparticles (C, D).

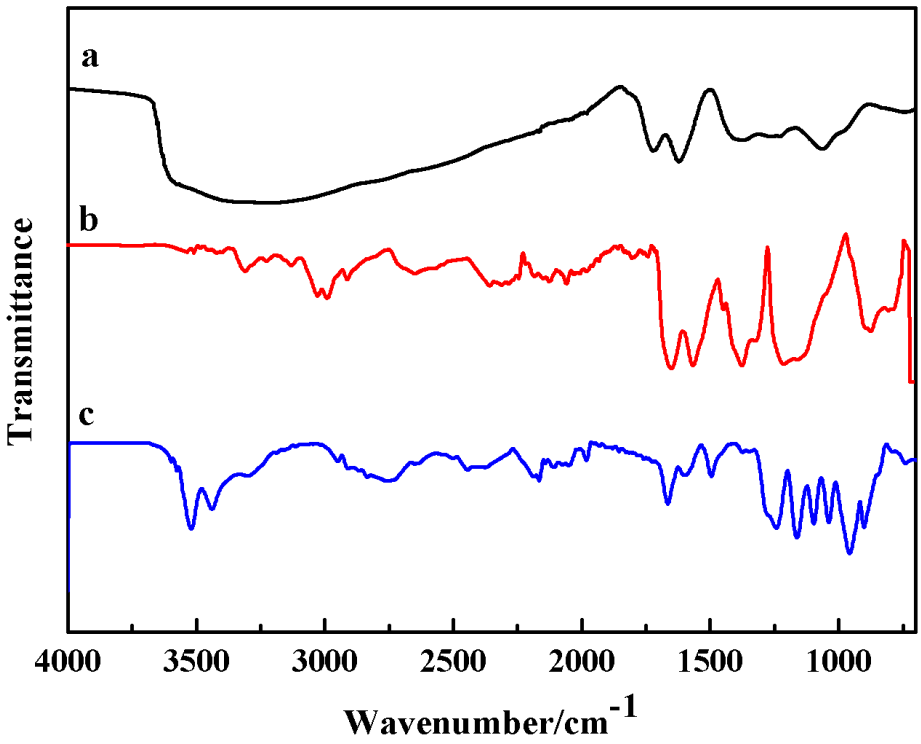


**Fig. 2** FTIR spectras of GO (a), GO-PANI (b) and G-PANI (c).

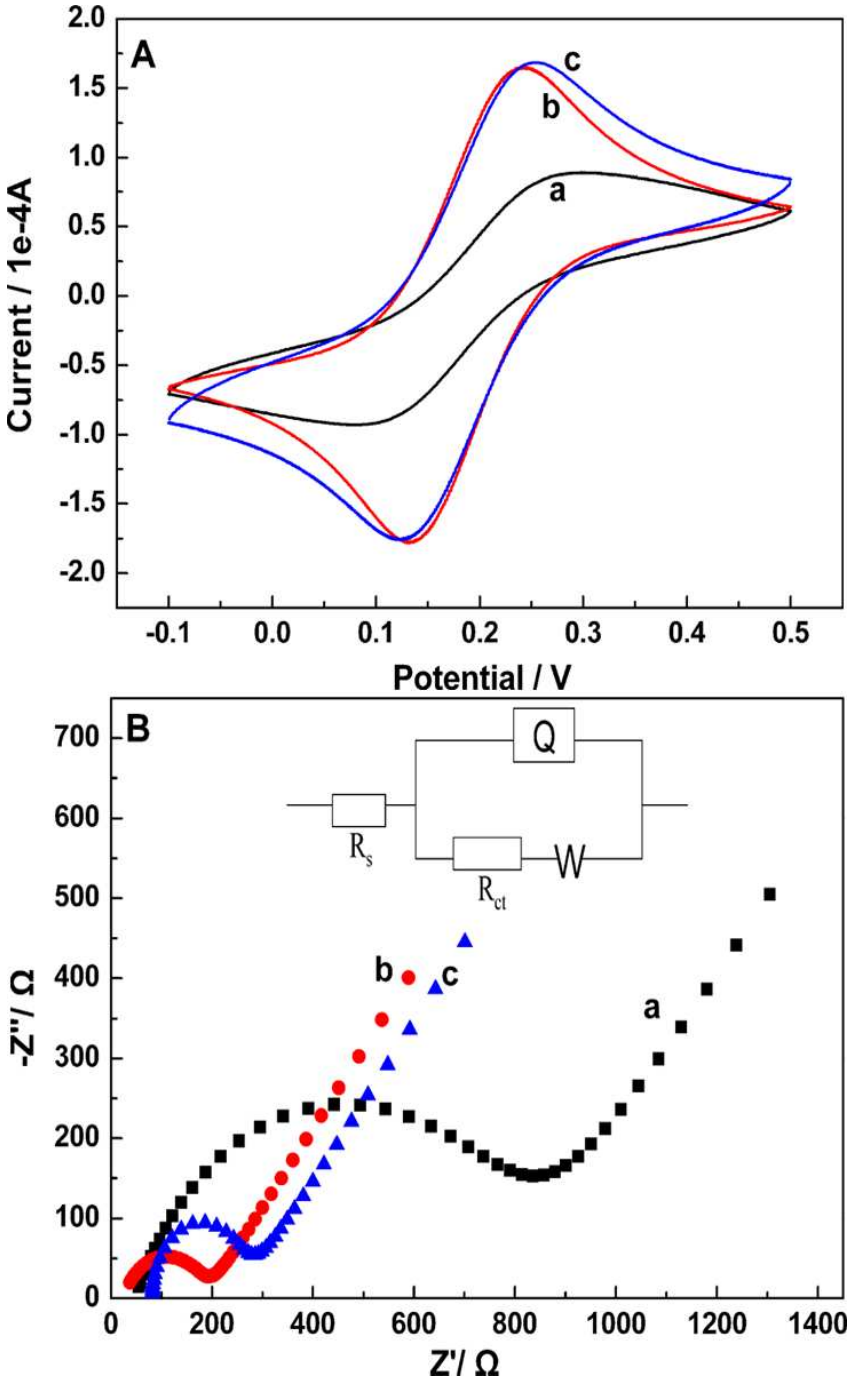


**Fig.3** (A) CVs of GCE (a), G-PANI/GCE (b) and Au-G-PANI/GCE (c) in 0.1 mol/L KCl containing 5 mmol/L $Fe[(CN)_6]^{3-/4-}$. (B) Nyquist plots of GCE (a), G-PANI/GCE (b) and Au-G-PANI/GCE (c) in 0.10 mol/L KCl containing 5 mmol/L $Fe[(CN)_6]^{3-/4-}$, and the inset shows the Randles equivalent circuit.

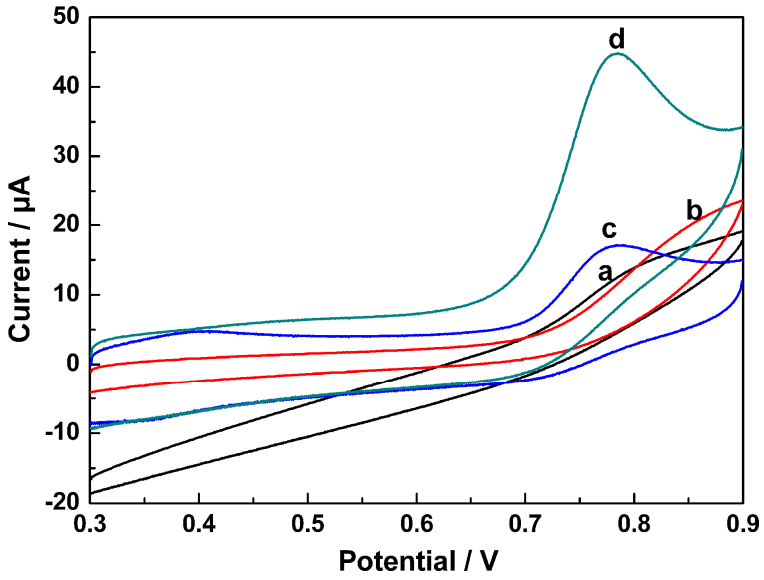


**Fig.4** CVs of GCE (a), G-PANI/GCE (b), Au/GCE (c) and Au-G-PANI/GCE (d) in 0.10 mol/L PBS with 0.10 mmol/L $NO_2^-$.

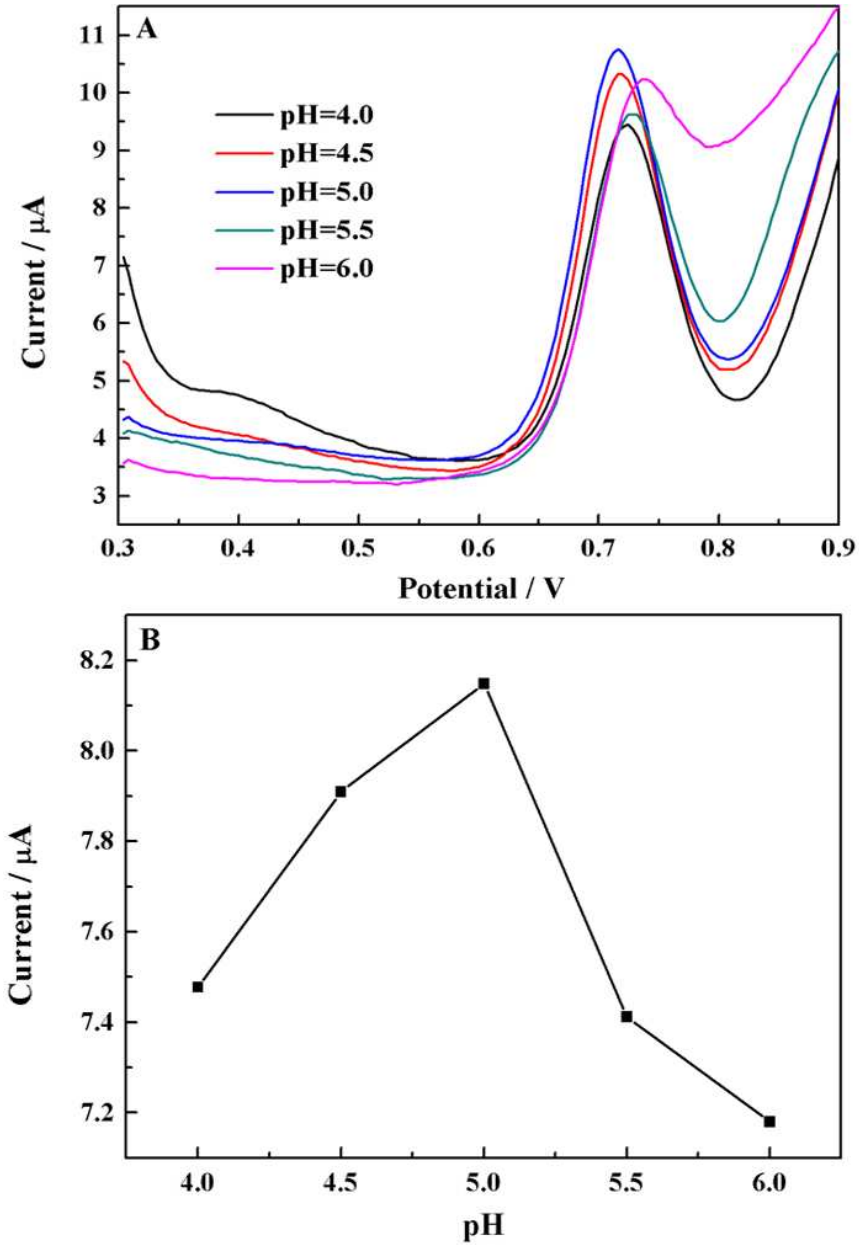


**Fig.5** (A) DPVs of Au-G-PANI/GCE in 0.10 mol/L PBS containing 0.10 mmol/L $NO_2^-$ at different pH values. (B) The relationship between the oxidation peak currents and the pH values.

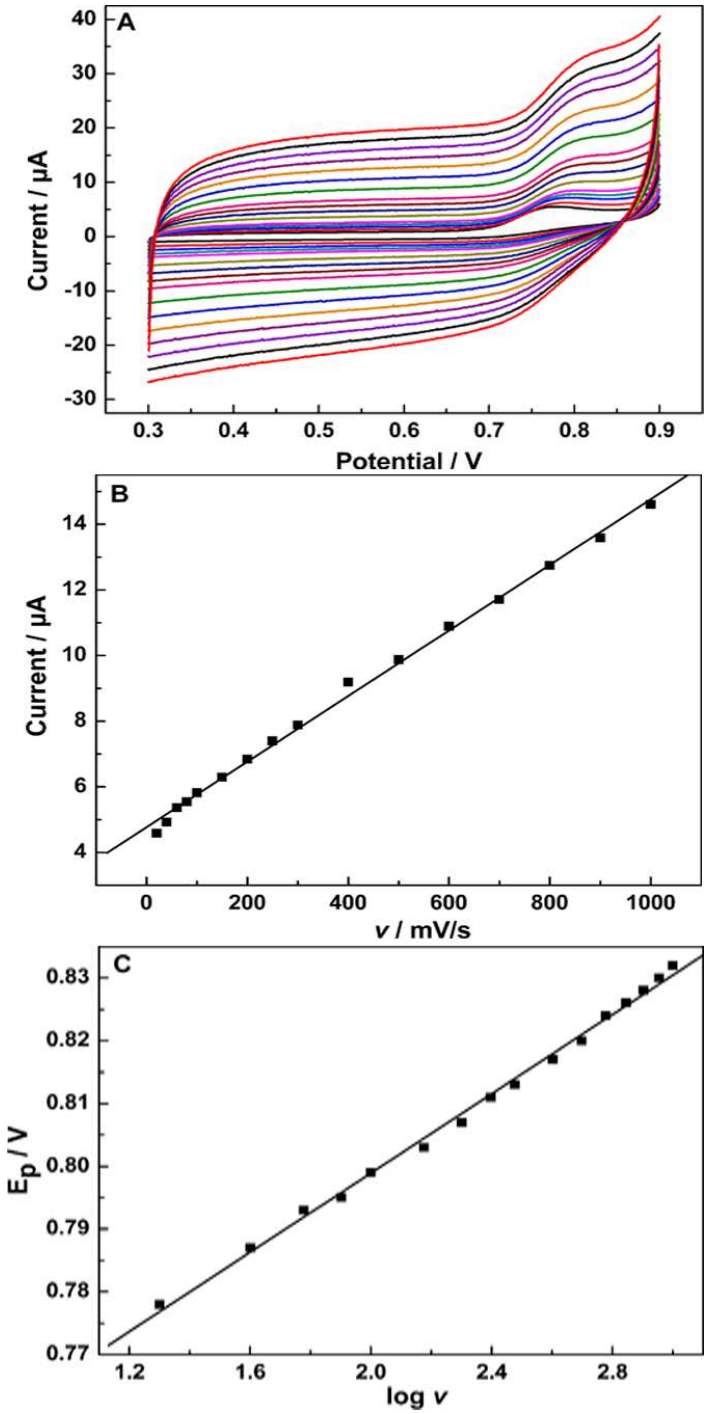


**Fig.6** (A) CVs of Au-G-PANI/GCE in 0.10 mol/L PBS (pH 5.0) containing 0.10 mmol/L $NO_2^-$ at different scan rates. (B) The linear dependence of $I_p$ on $v$. (C) The linear dependence of $E_p$ on log$v$.

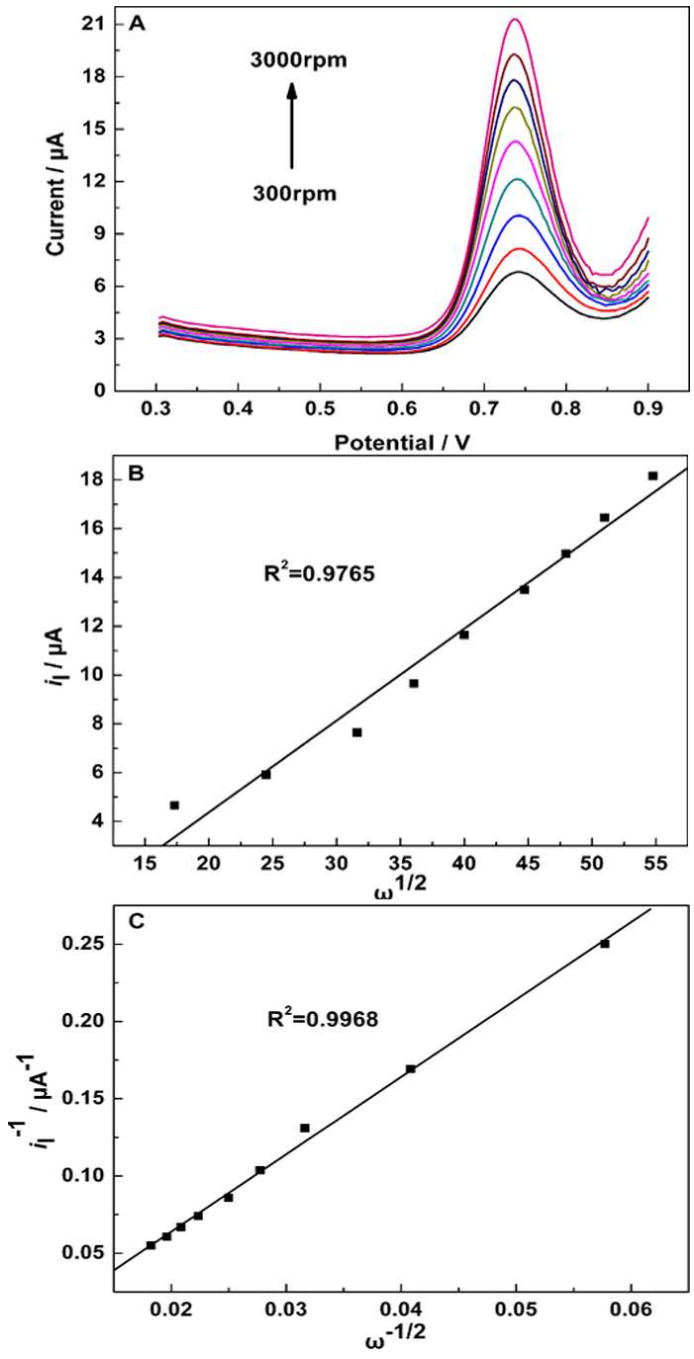


**Fig.7** (A) DPVs of Au-G-PANI/GCE RDE in 0.10 mol/L PBS (pH 5.0) containing 0.10 mmol/L $NO_2^-$ at different rotation rates. (B) The linear dependence of $i_l$ on $\omega^{1/2}$. (C) The linear dependence of $i_l^{-1}$ on $\omega^{-1/2}$.

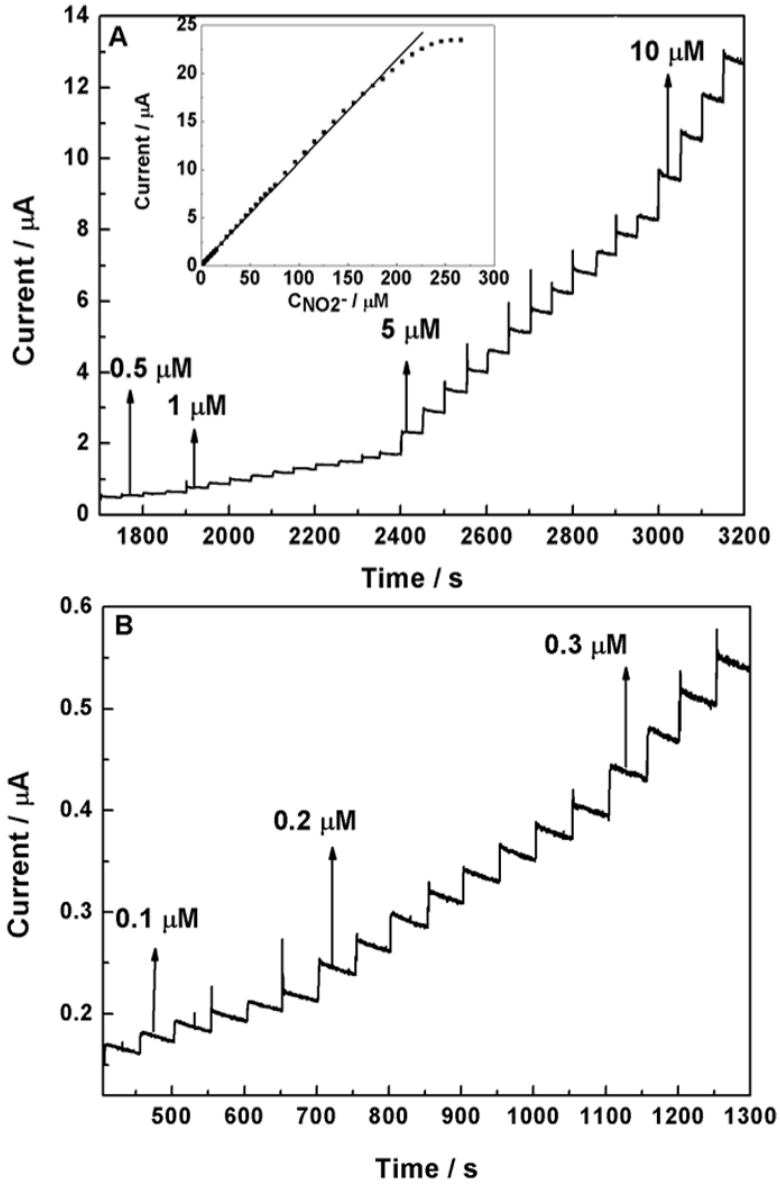


**Fig.8** (A) Amperometric response obtained on the Au-G-PANI/GCE with the increasing $NO_2^-$ concentration. Inset: The dependence of the current response on the concentration of $NO_2^-$. (B) The current response to low concentration $NO_2^-$ on Au-G-PANI/GCE. Supporting electrolyte: 0.10 mol/L PBS (pH 5.0), applied potential: +0.80 V.

**Table 1**

Performance comparison in the $NO_2^-$ detection between the as-fabricated Au-G-PANI/GCE and other electrodes.

| Electrode | Detection limit (μM) | Linear range (μM) | $R^2$ | References |
|---|---|---|---|---|
| Nafion/SLGnP–TPA–Mb/GCE | 10 | 50-250 | 0.9920 | [11] |
| Au@$Fe_3O_4$/Cys/GCE | 0.82 | 3.6-10000 | 0.9980 | [18] |
| nano-Au/P3MT/GCE | 2.3 | 10-1000 | | [19] |
| GR/PPy/CS/GCE | 0.1 | 0.5-722 | 0.9960 | [20] |
| Hb/Au modified electrode | 0.065 | 0.4-14.8 | 0.9982 | [26] |
| Nanometersized gold colloid/ethylenediamine/PGCE. | 45 | 130-44000 | 0.9984 | [27] |
| Au-G-PANI/GCE | 0.01 | 0.1-205.8 | 0.9986 | This work |

SLGnP–TPA–Mb: single-layer graphene nanoplatelet–protein composite film; Cys: L-Cysteine; P3MT: poly (3-methylthiophene); GR/PPy/CS: graphene/polypyrrole/chitosan nanocomposite.

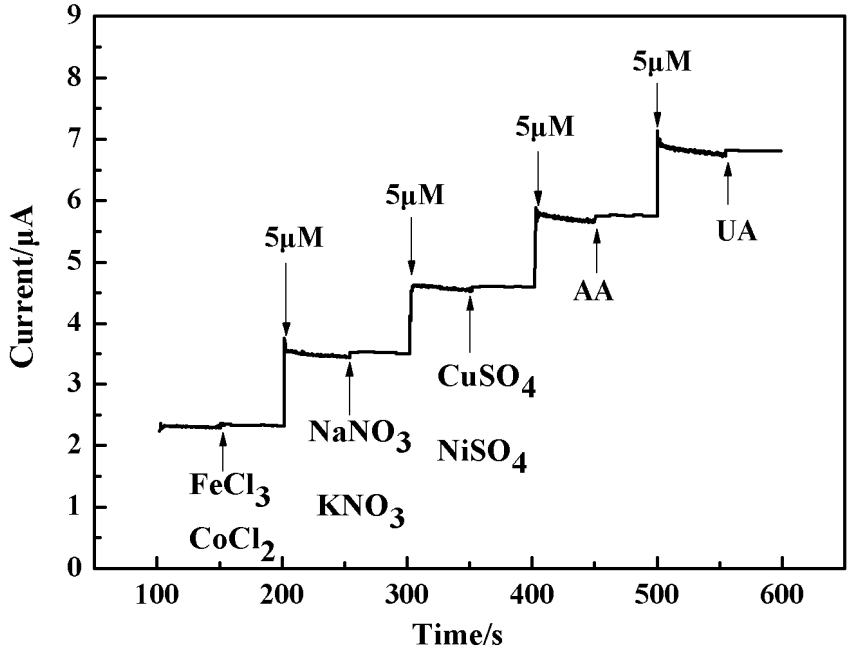


**Supplementary Information:** Possible interferences for the detection of $NO_2^-$ on the Au-G-PANI/GCE